Volume 19, Number 6 December 2013

Microscopy AND Microanalysis

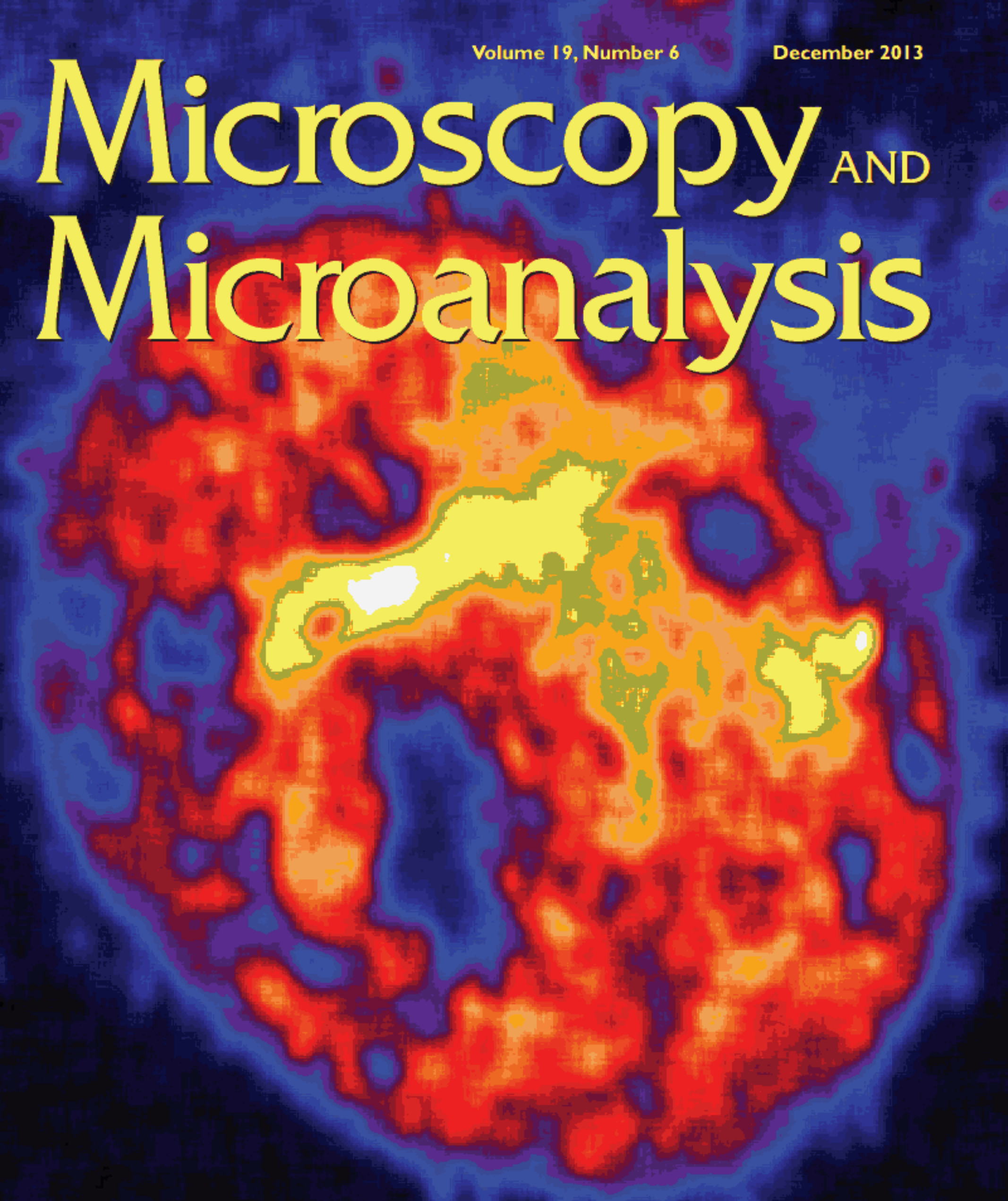

MSA
Microscopy Society of America

CAMBRIDGE
UNIVERSITY PRESS

ISSN 1431-9276

Microsc. Microanal. 19, 1490–1501, 2013
doi:10.1017/S1431927613013482

Microscopy AND Microanalysis

Correlated SEM, FIB-SEM, TEM, and NanoSIMS Imaging of Microbes from the Hindgut of a Lower Termite: Methods for *In Situ* Functional and Ecological Studies of Uncultivable Microbes

Kevin J. Carpenter,[1,*,†] Peter K. Weber,[1,*] M. Lee Davisson,[1] Jennifer Pett-Ridge,[1] Michael I. Haverty,[2] and Patrick J. Keeling[3]

[1]*Physical and Life Sciences Directorate, Lawrence Livermore National Laboratory, P.O. Box 808, L-231, Livermore, CA 94551, USA*
[2]*Division of Organisms and the Environment, Environmental Science, Policy and Management, University of California at Berkeley, 1301 South 46th Street, Building 478, Richmond, CA 94804-4698, USA*
[3]*Canadian Institute for Advanced Research, Department of Botany, University of British Columbia, 3529-6270 University Boulevard, Vancouver, BC V6T 1Z4, Canada*

Abstract: The hindguts of lower termites harbor highly diverse, endemic communities of symbiotic protists, bacteria, and archaea essential to the termite's ability to digest wood. Despite over a century of experimental studies, ecological roles of many of these microbes are unknown, partly because almost none can be cultivated. Many of the protists associate with bacterial symbionts, but hypotheses for their respective roles in nutrient exchange are based on genomes of only two such bacteria. To show how the ecological roles of protists and nutrient transfer with symbiotic bacteria can be elucidated by direct imaging, we combined stable isotope labeling (^{13}C-cellulose) of live termites with analysis of fixed hindgut microbes using correlated scanning electron microscopy, focused ion beam-scanning electron microscopy (FIB-SEM), transmission electron microscopy, and high resolution imaging mass spectrometry (NanoSIMS). We developed methods to prepare whole labeled cells on solid substrates, whole labeled cells milled with a FIB-SEM instrument to reveal cell interiors, and ultramicrotome sections of labeled cells for NanoSIMS imaging of ^{13}C enrichment in protists and associated bacteria. Our results show these methods have the potential to provide direct evidence for nutrient flow and suggest the oxymonad protist *Oxymonas dimorpha* phagocytoses and enzymatically degrades ingested wood fragments, and may transfer carbon derived from this to its surface bacterial symbionts.

Key words: bacteria, bioenergy, ecology, focused ion beam, SIMS, protists, scanning electron microscopy, stable isotopes, termites, transmission electron microscopy

Introduction

The microbial communities in the hindguts of lower termites and the closely related wood-feeding cockroach *Cryptocercus* (Lo et al., 2000; Inward et al., 2007) present numerous ecological, evolutionary, and cell biological/ultrastructural questions that have interested microbiologists for well over a century (Leidy, 1877; Grassi, 1917; Kirby, 1926; Cleveland et al., 1934; Hollande & Valentin, 1968; Radek et al., 1992; Hongoh et al., 2008*a*; Carpenter et al., 2010). In addition, hindguts of lower termites have proven to be a rich source of novel organisms with unexplored capabilities including numerous new protist, bacterial, and archaeal species and higher taxa, including novel bacterial phyla (Cleveland et al., 1934; Ohkuma & Kudo, 1996; Brugerolle & Lee, 2000*a*, 2000*b*; Hongoh et al., 2003; Stingl et al., 2004; Noda et al., 2006; Ohkuma et al., 2007; Ohkuma & Brune, 2011).

Received January 30, 2013; accepted August 20, 2013
*Corresponding author. kjcarpenter@lbl.gov; kevin@kevinjcarpenter.com; weber21@llnl.gov
†Current address: Life Sciences Division, Lawrence Berkeley National Laboratory, 1 Cyclotron Road, Mail Stop Donner, Berkeley, CA 94720, USA

The great efficiency with which these communities deconstruct wood lignocellulose into simple carbon compounds, fermentable sugars, and hydrogen gas (Ohkuma, 2003; Brune & Ohkuma, 2011) may hold potential for bioenergy applications. Working in concert with the termite's own limited cellulase activity in the jaw or midgut (Brune & Ohkuma, 2011), and often in symbiotic consortia (Hongoh et al., 2008*a*, 2008*b*), microbes in these communities carry out essential functions to allow their termite hosts to survive on a very nutrient poor diet of wood (Ohkuma, 2003). Many different lines of evidence indicate that large, structurally complex, anaerobic flagellate protists of the phylum Parabasalia, and likely some members of the order Oxymonadida, are responsible for phagocytosis and enzymatic degradation of wood fragments ingested by the termite (Cleveland et al., 1934; Yamin, 1981; Nakashima et al., 2002; Kiuchi et al., 2004). Bacterial diversity in lower termite hindguts is very high, with as many as 700+ phylotypes representing 15 bacterial phyla (commonly, Spirochetes, Firmicutes, Bacteroidetes, Elusimicrobia) present in a single hindgut (Ohkuma & Brune, 2011). However, most prokaryotic cells are found in association with a protist rather than free swimming

(Berchtold et al., 1999; Noda et al., 2005). A single protist cell may harbor up to 10^5 such bacterial symbionts (Noda et al., 2005) on its cell surface and/or within cytoplasmic vesicles (Cleveland & Grimstone, 1964; Bloodgood & Fitzharris, 1976; Radek et al., 1992; Noda et al., 2005; Brune & Stingl, 2006; Carpenter et al., 2011). Genomes of two novel bacterial species found in association with large cellulolytic parabasalid protists suggest that they may play a role in nitrogen metabolism, both in fixation of N_2 and in the synthesis and provisioning the protist host with amino acids and cofactors, in return for glucose from lignocellulose degradation by the protist (Hongoh et al., 2008*a*, 2008*b*). The presence of nitrogenase gene (nifH) homolog and evidence for uptake of $^{15}N_2$ by cultures of the spirochete *Treponema* (from the hindgut of the lower termite *Coptotermes formosanus*) suggest that these spirochetes are responsible for fixation of atmospheric dinitrogen gas (Lilburn et al., 2001).

Although numerous experimental and molecular approaches have yielded functional hypotheses for some of the microbes in hindguts of lower termites (Cleveland, 1925; Yamin, 1981; Leadbetter et al., 1999; Nakashima et al., 2002; Kiuchi et al., 2004; Hongoh et al., 2008*a*, 2008*b*), these organisms represent only a small fraction of the whole. In the case of metabolite exchange occurring in protist–bacterial symbioses, current hypotheses are based on genomes of two bacterial species symbiotic with two species of large, parabasalid protists (Hongoh et al., 2008*a*, 2008*b*). Very little data exist on what role the smaller species of parabasalia and most oxymonad species play in these systems, and currently little data exist with bearing on metabolite exchange between these protists and their bacterial symbionts. In part, this lack of data is due to the difficulties in cultivating these protists and examining their ecological functions individually.

Conceptually, stable isotope tracing should offer a promising and noninvasive method to infer the roles of both protists and bacterial symbionts in the lower termite hindgut, thereby linking their identity to function. With this culture-independent approach, the entire microbial community is exposed *in situ* to a substrate highly enriched in a rare stable isotope (typically ^{13}C or ^{15}N), and this label is then followed into specific members of a microbial community via isolation of enriched DNA, RNA, lipids, or whole cells (Boschker et al., 1998; Radajewski et al., 2000; Manefield et al., 2002; Mayali et al., 2012; Pett-Ridge & Weber, 2012). Typically, organisms that have incorporated high levels of the rare isotope are interpreted to be using the substrate, although the potential for some organisms to become labeled by feeding on metabolites from the primary users of the substrate (cross feeding) must be considered, particularly with long incubation times (Murrell & Whiteley, 2011). Recent advances in imaging mass spectrometry applied to microbial systems have taken this approach to the single cell level in pure cultures and complex microbial communities (Lechene et al., 2006; Behrens et al., 2008; Musat et al., 2008; Woebken et al., 2012).

High resolution (cellular and sub-cellular level) imaging mass spectrometry (e.g., NanoSIMS) generally requires the same sample fixation and preservation standards as scanning electron microscopy (SEM). In addition to being fixed, fully dehydrated, and electrically conductive, cells must also be stable in high vacuum environments for interrogation by high energy beam sources. Due partly to interest in their often highly complex and unusual morphologies, the protists of lower termite hindguts have been the subject of many investigations with light and transmission electron microscopy (TEM) (Grassi, 1917; Koidzumi, 1921; Kirby, 1932; Cleveland & Grimstone, 1964; Hollande & Carruette-Valentin, 1971; Radek et al., 1992; Brugerolle & Lee, 2000*a*, 2000*b*; Brugerolle & Bordereau, 2004; Stingl et al., 2004; Carpenter et al., 2008). However, until recently, studies of their surface morphology with SEM played only a limited role and appeared in far fewer studies (Radek et al., 1992; Leander & Keeling, 2004; Stingl et al., 2004; Noda et al., 2006). More recently, Carpenter & Keeling (2007) established a fixation method for hindgut protists of termites and *Cryptocercus*, which, combined with high resolution field emission SEM, revealed previously unknown bacterial surface symbionts, ultrastructural features, and provided evidence to formulate new hypotheses about functional morphology and phenotypic character evolution in these groups (Carpenter & Keeling, 2007; Carpenter et al., 2008, 2009, 2010, 2011).

Here we report a set of robust methods to directly investigate the ecological relationships between the protists and bacterial surface symbionts using *in situ* stable isotope labeling of live termites and subsequent imaging of fixed hindgut microbes by electron microscopy (SEM, FIB-SEM, and TEM) and high resolution imaging mass spectrometry with a NanoSIMS 50 (Cameca, Gennevilliers, France). We focused our efforts on a common and readily identifiable protist species with a covering of bacterial surface symbionts. Based on our observations with SEM and TEM, we found the oxymonad protist *Oxymonas dimorpha* Connell was best suited for this purpose. For sample preparation, we (1) produced whole protist and bacterial cells on solid substrates, which were directly imaged by SEM and analyzed by NanoSIMS; (2) sectioned the intact *O. dimorpha* cells with a focused ion beam-scanning electron microscope (FIB-SEM) instrument to reveal internal structure for NanoSIMS analysis; and (3) prepared ultramicrotome sections for TEM and NanoSIMS analysis. Imaging with SEM or TEM was carried out to identify targets and correlate cell ultrastructural and surface morphological features with NanoSIMS imaging. Following a 6-week stable isotope labeling experiment, results for the three approaches were compared and used to formulate hypotheses for the role of *O. dimorpha* in cellulose metabolism and carbon transfer to its bacterial symbionts.

Materials and Methods

Stable Isotope Labeling with ^{13}C Cellulose

Portions of three colonies of *Paraneotermes simplicicornis* Banks (common name: desert dampwood termite) in the family Kalotermitidae were collected from a naturally occur-

ring population. These colonies were located in partially buried dead limbs of desert trees (*Acacia greggii* A. Gray) along a wash in the northern portion of Tucson, Arizona. Pseudergates (a worker-like caste described by Miller, 1969) and soldiers were removed from the wood, placed in plastic boxes (17 × 12 × 6.5 cm), provisioned with small pieces of *A. greggii* and sufficient moisture, and transported to Lawrence Livermore National Laboratory. They were housed in the laboratory in the same plastic boxes in the dark at room temperature (~20°C).

In an attempt to maximize the probability of detecting ^{13}C enrichment across all members of the hindgut microbial community, we chose a 6 week labeling duration (exposure to ^{13}C-enriched cellulose). For this experiment, six pseudergates were placed in a 150 mL glass serum vial with sufficient moisture and ~50 mg of ^{13}C-enriched cellulose (97 at%, Isolife) as their sole food source. This feeding substrate is certified to comprise only ^{13}C-labeled (and unlabeled) cellulose and no other carbon compounds. The vial was wrapped in aluminum foil to simulate the termites' natural dark environment, and the termites were visually inspected weekly. The termites were left in the vial for a total labeling duration of 6 weeks before removal and dissection.

In addition to the 6-week exposure, we performed a control experiment to determine the natural abundance $^{13}C/^{12}C$ ratio across a range of protist diversity and topographies in fixed whole cells. Several *P. simplicicornis* pseudergates were taken directly from the wood in which they were collected with no exposure to isotopically enriched compounds. This material was fixed with the same method used for labeled termites (below). We analyzed four protist species to cover a range of taxonomy and topography. These included the parabasalids *Hoplonympha natator* Light (analyses of both surface bacteria and protist flagella), *Kofoidia loriculata* Light (analyses of both the protist cell body with bacteria and protist flagella), a member of class Spirotrichonymphea (*Spironympha polygyra* Cupp or *Spirotrichonympha bispira* Cleveland), and the oxymonad *O. dimorpha*. One or two individual cells were analyzed for each species.

Cell Fixation and Preparation Methods for SEM, FIB-SEM, TEM, and NanoSIMS

Hindgut contents of both labeled and unlabeled (control group) pseudergates were fixed chemically, which provided material for examination/analysis with four different imaging modalities: whole cells for SEM and FIB-SEM (for *in situ* top-cuts), as well as embedded, ultramicrotome sectioned material for TEM, all of which was imaged with NanoSIMS.

Before dissection *P. simplicicornis* pseudergates were removed from enclosures by emptying them onto Petri dishes. Termites that had been fed ^{13}C cellulose were separated from pieces of this material and termite fecal matter with microdissection tools to as great a degree as possible. To dislodge and remove any remaining adherent ^{13}C cellulose or fecal matter, termites were gently picked up with forceps and rinsed by brief (5 s) immersion in Trager Medium U buffer (Trager, 1934). To obtain hindgut fluid, termites were dissected by using forceps to pull out the gut by grasping the posteriormost segment of the abdomen. This was immediately immersed in a drop of Trager Medium U buffer in a Petri dish and cut open to release hindgut contents. Approximately 250 μL of hindgut contents in buffer were pipetted into a 1.5 mL plastic tube containing 750 μL of 3% v/v glutaraldehyde (diluted in Trager Medium U buffer) to yield a final glutaraldehyde concentration of 2–2.5%. Hindgut contents were allowed to fix for 30 min, and tubes were gently inverted by hand approximately every 10 min to ensure adequate mixing. After primary fixation, tubes were centrifuged for 10 s and the supernatant was extracted with a pipette. Trager Medium U buffer was added as a rinse. This rinse was repeated, and then cells were postfixed in 1% v/v OsO_4 for 30 min and resuspended in buffer. Fixed material in buffer was then split into two approximately equal portions—one for embedding and sectioning for TEM and NanoSIMS analysis of thin sections, and one for SEM and NanoSIMS analysis of whole cells and cells milled with a FIB-SEM instrument.

Preparation Method 1: Whole Cells for SEM and/or NanoSIMS

Fixed material in buffer was pipetted onto a 13 mm diameter Isopore membrane filter (Millipore, Billerica, MA, USA) with 1 or 3 μm pore size held in a Millipore Swinnex plastic cartridge between two Millipore teflon rings. Care was taken not to introduce too much of the fixed material onto the filters. Otherwise, the pores can become clogged, resulting in pressure imprints and undulations in the filter that hinder effective NanoSIMS analysis of material on the filters. Immediately after fixed material was introduced over the filter, the ethanol dehydration series was begun by attaching a 10 mL syringe with Luer lock filled with 50% ethanol to the cartridge, expelling about half of the ethanol, and allowing fixed cells to dehydrate for 10 min. This process was repeated with 70, 90, and two changes of 100% ethanol. Carbon dioxide critical point drying was carried out with an Auto Samdri 815 critical point dryer (Tousimis, Rockville, MD, USA). Critical point-dried filters were affixed to 10 or 13 mm aluminum SEM stubs with carbon double stick tape, and sputter coated with 5 nm of iridium using a 208HR sputter coater (Cressington, Watford, UK). Material was examined and targets for NanoSIMS were selected and mapped with a 7401F FESEM (JEOL, Tokyo, Japan) or an Inspect F SEM (FEI, Hillsboro, OR, USA). Samples were typically examined at low accelerating voltage (5 kV or less) to minimize charging, and moderately long working distance (8–28 mm) to improve depth of field. Protist morphology was matched to published descriptions while consulting Yamin (1979) as a guide to identification.

Preparation Method 2: FIB-Sectioned Whole Cells

Four whole cells of the oxymonad protist *O. dimorpha* from the mapped samples were selected for FIB sectioning using a top-cut method (Weber et al., 2010). FIB top-cuts were made with an Nova 600i DualBeam FIB/SEM (FEI) at

Table 1. Protocol for Ethanol Dehydration and LR White Infiltration, Embedding, and Polymerization with the Pelco Biowave Microwave.

Treatment	Time	Temperature (°C)	Power Level	Vacuum
Dehydration				
30% ethanol	40 s	35	1	No
50% ethanol	40 s	35	1	No
70% ethanol	40 s	35	1	No
90% ethanol	40 s	35	1	No
100% ethanol	3 × 40 s	35	1	No
Embedding				
30% LR White*	4 min	35	1	Yes
50% LR White	4 min	35	1	Yes
70% LR White	4 min	35	2	Yes
90% LR White	4 min	35	3	Yes
100% LR White	3 × 4 min	45	3	Yes
Polymerization				
100% LR**	45 min	80	6	No

*LR White is dissolved in 100% ethanol.
**See the Materials and Methods section for more details.

LLNL. The SEM stub surface was oriented within ~20° parallel to the ion beam axis. A 30 kV Ga^+ FIB with a current of 0.28 nA was used for cutting. SEM images were used to locate targets in the NanoSIMS.

Preparation Method 3: Resin-Embedded Cells for TEM and NanoSIMS

Material for TEM was dehydrated with ethanol and embedded in L.R. White acrylic resin using a Biowave microwave (Pelco, Redding, CA, USA) following the protocol of Giberson et al. (1997) described in Table 1. After material was infiltrated with 100% acrylic, it was transferred to a flat-bottomed plastic capsule, covered with fresh acrylic, and the top of the capsule was covered with parafilm. The capsule lid was placed over the parafilm, and the capsule as submerged in water for the duration of the polymerization (Table 1). An EM UC6 ultramicrotome (Leica, Wetzlar, Germany) was used to section embedded material to an initial thickness of 1 μm to check for the presence of suitable *O. dimorpha* targets. This was done by staining sections with toluidine blue followed by examination with light microscopy (LM). Upon identification of appropriate cell targets, sections for imaging with TEM and NanoSIMS were cut at 100–200 nm. Ultrathin sections (i.e., 60–80 nm) are typically too thin for NanoSIMS analysis; a thicker section in the 100–200 nm range is desirable to extend analysis time under primary ion beam sputtering. Sections were placed on formvar and carbon-coated copper mesh grids, and examined and mapped for NanoSIMS with a transmitted electron detector in a 7401F FESEM (JEOL) in STEM mode at 30 kV.

NanoSIMS Analysis

High-resolution imaging secondary ion mass spectrometry (SIMS) was performed using a NanoSIMS 50 (Cameca) at LLNL. Samples were examined with a Cs^+ primary ion beam, which enhances the production of negatively charged secondary ions. Primary beam current at the sample ranged from 2–4 pA. Carbon isotopes were collected as monomers ($^{12}C^-$ and $^{13}C^-$), or as dimers ($^{12}C_2^-$ and $^{12}C^{13}C^-$). Most analyses, including those for material prepared by all three methods, ranged between 5 and 40 μm raster with ~150 nm lateral resolution using a primary aperture (D1) of 300 μm and a primary lens (L1) setting of zero. Three whole *O. dimorpha* cells were selected for successive analyses at increasing depths in the cell—a form of depth profile analysis. To carry this out, a first analysis was taken at the cell surface, then the same analysis area was sputtered at an increased rate using a higher primary beam current (also called burn-in) to penetrate deeper into the sample. This combination of analysis and burn-in was repeated to give three to five analyses at increasing depths, starting from the surface for a given cell. High primary beam current sample sputtering was done with L1 at 1,750 and a 750 μm D1 aperture to achieve ~0.5 nA at the sample for 60–240 s to penetrate inside the cell. The mass spectrometer was tuned to achieve a mass resolving power of at least 7,000, which is necessary for distinguishing isobaric interferences (e.g., at mass 25 distinguishing $^{13}C^{12}C^-$ from $^{12}C_2H^-$). Imaging data were processed using custom software (LIMAGE, L. Nittler, Carnegie Institution of Washington). For whole cell analyses, ratio data were extracted from regions of interest (ROIs) drawn for the entire subregion of the analyzed cell. For sectioned cells, the data were extracted for the protist interior separately from the adhering bacteria. Data are presented both as ratios and at% enrichment (Popa et al., 2007):

$$\mathrm{APE} = [R_f/(R_f + 1) - R_i/(R_i + 1)] \times 100\%,$$

where R_f is the measured ratio ($^{13}C/^{12}C$) and R_i is the initial ratio ($^{13}C/^{12}C$). For the latter, we use the average ratio for the control analyses, which reflects the initial gut community isotopic composition and corrects for instrumental mass fractionation (≃4% in these analyses). Measurement variability is reported as one standard deviation (SD) for reference measurements and one standard error (SE) for unknowns.

Results

Fixation for Whole Cells and Thin Sections for SEM, TEM, and NanoSIMS

Protists from isotopically labeled or unlabeled termites fixed with glutaraldehyde and osmium tetroxide generally remained fully intact and retained their overall shape without distortion (Figs. 1A–1G). Membranes retained their integrity (except for slight tearing which is common, especially on larger cells), while flagella, surface symbiotic bacteria, and other features were well preserved with little or no damage, and remained largely free of debris (Figs. 1A–1G). We observed very few protists that had been damaged extensively enough to preclude at least tentative identifica-

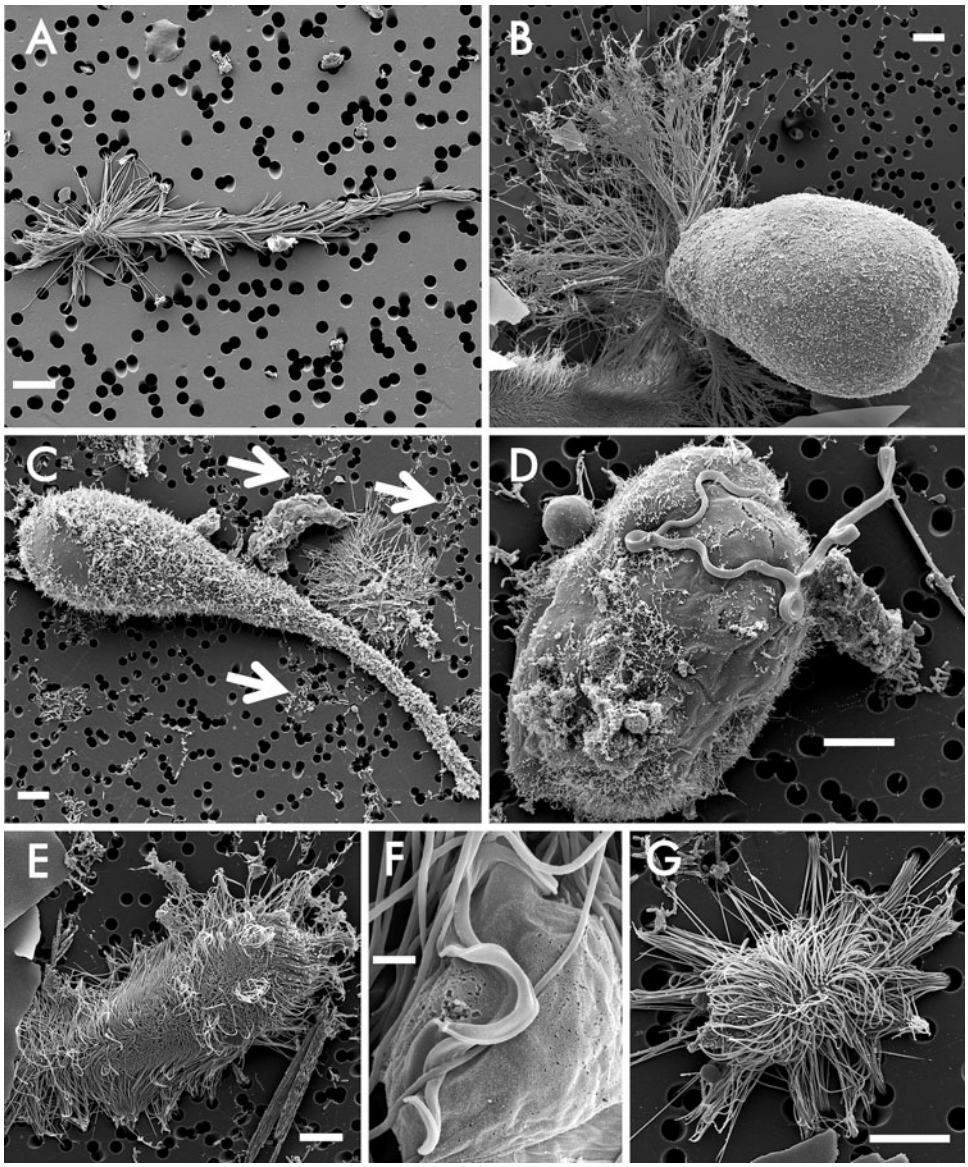

Figure 1. Scanning electron microscopy micrographs of protists from the hindgut of the lower termite *Paraneotermes simplicicornis*: (**A**) *Hoplonympha natator* (Parabasalia); (**B**) *Kofoidia loriculata* (Parabasalia); (**C**) *Oxymonas dimorpha* (Oxymonadida), free swimming bacteria at arrows; (**D**) *Foaina taeniola* (Parabasalia); (**E**, **G**) unidentified members of the parabasalid group Spirotrichonymphaea, likely *Spirotrichonympha bispira* (**E**) and *Spironympha polygyra* (**G**); (**F**) an unidentified parabasalid, likely *Trichomonas* sp. Scale bar: (**A**–**E**, **G**) 10 μm, (**F**) 1 μm.

tion to the genus level. Based on SEM observations of this fixed material, using Yamin (1979) and Brugerolle and Lee (2000*a*, 2000*b*) as references, we were able to unequivocally identify three protists to the species level: the parabasalids *H. natator*—an elongate, tapering cell ~100 μm in length with two distinct anterior flagellar regions, and completely covered elsewhere by elongate surface bacteria (Fig. 1A); *K. loriculata*—a spheroidal cell ~60–140 μm in length with several distinct anterior flagellar bundles (loricula) and a covering of surface bacteria of varying density (Fig. 1B); and the oxymonad *O dimorpha*—a large cell (~50–200 μm) varying between club-shaped forms with a thinner, elongate anterior rostellum, and spheroidal forms, both bearing a typically dense covering of surface bacteria (Fig. 1C). It was also possible to tentatively identify other smaller parabasalid protists to the species or genus level including: *Foaina taeniola*—a rounded to ellipsoidal cell with a thickened recurrent flagellum and a typically uneven complement of surface bacteria (Fig. 1D), and an undescribed, small parabasalid—possibly, *Trichomonas* spp.—based on its small size and undulating membrane (Fig. 1F). Cells conforming to the description of *Spirotrichonympha bispira* and *Spironympha polygyra*—both with numerous flagella undergoing helical coiling along the length of the cell body—were also commonly observed, and were generally well preserved. However, it was not possible to unequivocally distinguish them (Figs. 1E, 1G). Ultramicrotome-cut thin sections showed adequate contrast (without poststaining) and good structural preservation, with intact membranes, and well-preserved organelles and surface bacterial symbionts (Fig. 3A).

NanoSIMS Analysis of Whole Cells

Measurements of unlabeled control samples were performed to provide a reference for the labeling experiment and to test for topographical effects of the large cells. The mean $^{13}C/^{12}C$ ratio for four different protist species (including the oxymonad *O. dimorpha* and the parabasalids *K.*

loriculata, *H. natator*, and an unidentified spirotrichonymphid) was 0.01057 ± 0.00018 SD (^{13}C APE ≡ 0; Fig. 4). While the variability observed in these measurements was high relative to counting statistics for the measurements (~2 versus ~0.1%), the precision was sufficient for this tracer study. These data do not include analyses of cells that had poor ion yield because of charging or extraction field distortion. With a diameter of roughly 100 μm and a generally spheroidal cell shape (Fig. 1B), *K. loriculata* had the most extreme topography of any cell type in this termite, and ion and secondary electron shadows were frequently observed associated with it during NanoSIMS imaging.

NanoSIMS surface analysis of 11 whole *O. dimorpha* cells from *P. simplicicornis* isotopically labeled for 6 weeks on ^{13}C cellulose showed ~50-fold ^{13}C enrichment above natural abundance, with a mean ^{13}C/^{12}C ratio of 0.48 ± 0.056 SE (^{13}C APE = 31%; Fig. 4). Three of these 11 cells were chosen for depth profile analysis that included between two and four additional analyses (see the Materials and Methods section). In two of three cells, enrichment of ^{13}C remained roughly constant, and in the third cell, ^{13}C enrichment decreased with depth, but we were not able to verify that any of the depth profile result represented the interior of the protist. The sputter craters were observed to develop significant topography after a couple of cycles of high-current sputtering, and it was not clear from postanalysis SEM imaging whether the bacteria were fully removed even after sputtering with an intensity that would nominally result in a crater 5–10 μm deep. Differential sputtering also resulted in some areas becoming so deep that ion yield fell off dramatically, making the results suspect.

NanoSIMS Analysis of FIB-Milled Whole Cells

The interiors of four *O. dimorpha* cells from *P. simplicicornis* labeled for 6 weeks were exposed with a top-cut by a FIB Ga^+ ion beam and these were subsequently reimaged with SEM and analyzed with NanoSIMS. All four cells retained their overall shape and integrity (Figs. 2A, 2C), and are readily identified as *O. dimorpha* due to their overall cell size and shape, and particularly due to their distinctive surface appearance that is the result of numerous circular invaginations associated with pinocytosis, and well characterized in several oxymonads (Rother et al., 1999; Maaß & Radek, 2006; Carpenter et al., 2008). The interior of the cells revealed by this process showed heterogeneity in ^{13}C enrichment with very highly enriched areas (e.g., ^{13}C/^{12}C ratios of 4:1 or higher or ^{13}C APE > 74%) surrounded by areas of lower enrichment (Figs. 2B, 2D). In two cells, material contained within what appeared to be a large (~10 μm) phagosomal membrane showed very high ^{13}C enrichment (Figs. 2C, 2D, arrows). The overall level of ^{13}C enrichment observed in the cell interior of FIB-sectioned cells was by far the highest of the three preparation methods, with a mean value of 1.1 ± 0.16 SE (^{13}C APE = 51%), which is more than double that observed in whole cells (Fig. 4).

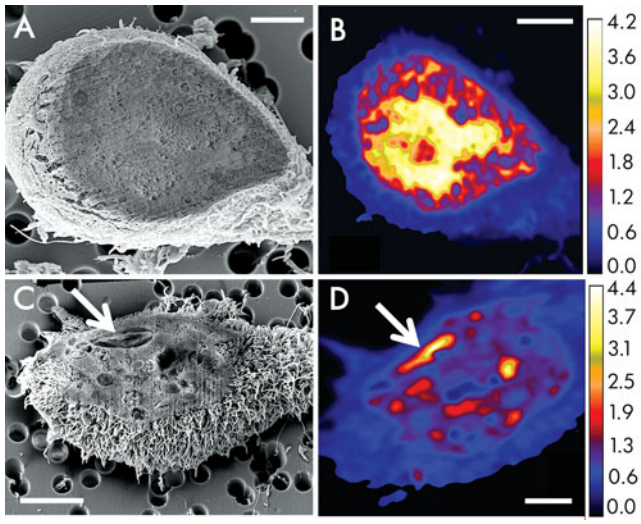

Figure 2. NanoSIMS ion micrographs showing levels of ^{13}C enrichment (^{13}C/^{12}C) with corresponding scanning electron microscopy micrographs of *Oxymonas dimorpha* cells (natural ^{13}C/^{12}C ≃ 0.01): (**A**, **B**) cell with FIB-milled surface; (**C**, **D**) FIB-milled cell showing a highly enriched particle inside a phagosomal membrane (arrows). Scale bar is 5 μm.

NanoSIMS Analysis of Resin-Embedded Thin Sections

Before cutting thin sections of acrylic-embedded gut material from *P. simplicicornis* (labeled for 6 weeks) for TEM and NanoSIMS, thicker sections (~1 μm) from the same region of the block were cut, stained with toluidine blue, and examined with LM. These images showed numerous clusters of several to dozens of *O. dimorpha* cells attached to pieces of the termite hindgut wall. The elongate rostellum of many of these *O. dimorpha* cells was seen in section attached to the gut wall. This feature is not present in any other protist species known from *P. simplicicornis*, including *K. loriculata*, a cell that may be confused with *O. dimorpha* in section. (An *O. dimorpha* cell in section not showing the rostellum would have approximately the same rounded shape and bacterial surface symbionts as a *K. loriculata* cell.) The rostellum is seen pointing to the upper right hand corner in the images of the *O. dimorpha* cell in Figure 3 (see bracket), and in other cells analyzed by TEM and NanoSIMS. In addition, the cells also display the distinctive surface invaginations characteristic of oxymonads and unknown in parabasalia (Fig. 3A). Taken together, we are confident that the LM, TEM, and NanoSIMS images indicate that all five cells we analyzed were indeed *O. dimorpha* and not *K. loriculata* or some other species.

The *O. dimorpha* cells we analyzed from thin secions showed ~10-fold ^{13}C enrichment above the initial composition (mean ^{13}C/^{12}C ratio of 0.10 ± 0.0040 SE; ^{13}C APE = 8%; Figs. 4, 5). As with the interiors of cells revealed by FIB top-cut, we observed intracellular heterogeneity of ^{13}C enrichment corresponding to ultrastructural features seen in electron microscope imaging (see unidentified round organelle in Fig. 3). However, overall enrichment of the *O. dimor-*

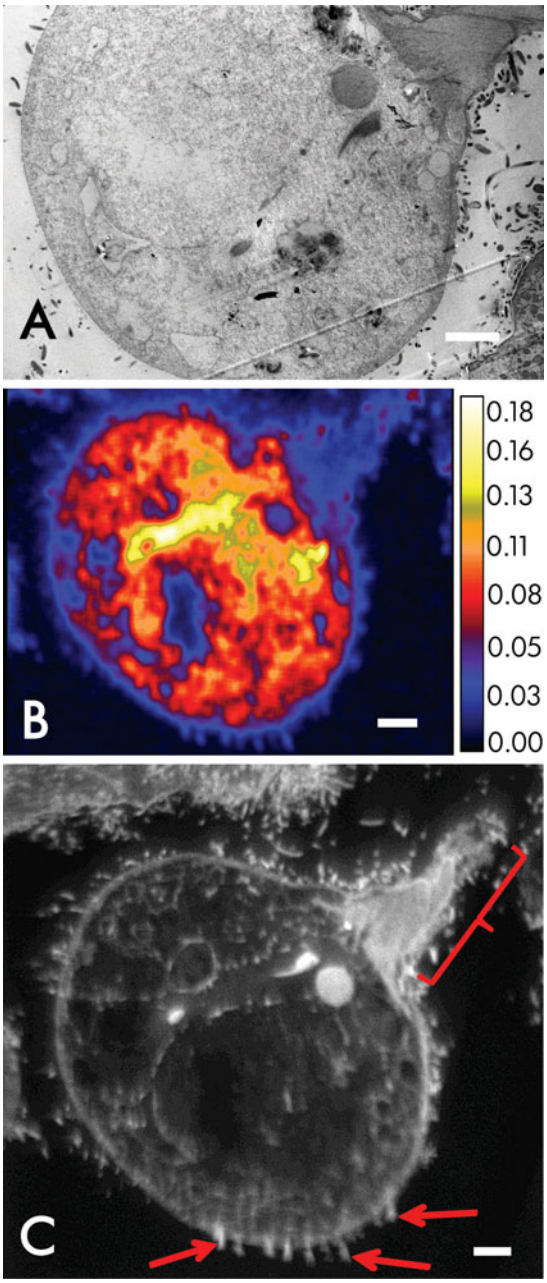

Figure 3. Transmission electron microscopy micrograph and corresponding NanoSIMS ion micrographs of an *Oxymonas dimorpha* cell in thin section: (**A**) TEM micrograph; (**B**) NanoSIMS ion micrograph showing levels of ^{13}C enrichment ($^{13}C/^{12}C$) (natural abundance of $^{13}C/^{12}C = 0.01$); (**C**) NanoSIMS ion micrograph showing $^{12}C^{14}N^-$ secondary ion counts. Gray levels correspond to counts of this ion, with the fewest counts depicted in black and the most in white. Bracket indicates the rostellum, a distinctive morphological feature of *O. dimorpha* among the *Paraneotermes simplicicornis* hindgut biota. Arrows indicate typical attached surface bacteria. Scale bar is 5 μm.

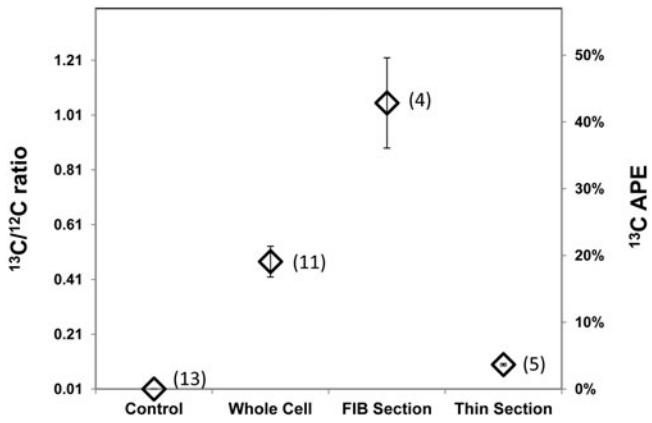

Figure 4. Comparison of ^{13}C enrichment ($^{13}C/^{12}C$ ratios and ^{13}C APE) from *Oxymonas dimorpha* cells prepared by three different methods, and controls consisting of four different protist species from unlabeled termites (see the Materials and Methods section). Error bars represent standard error of the mean for each method. Numbers in parentheses indicate the number of cells analyzed for each method.

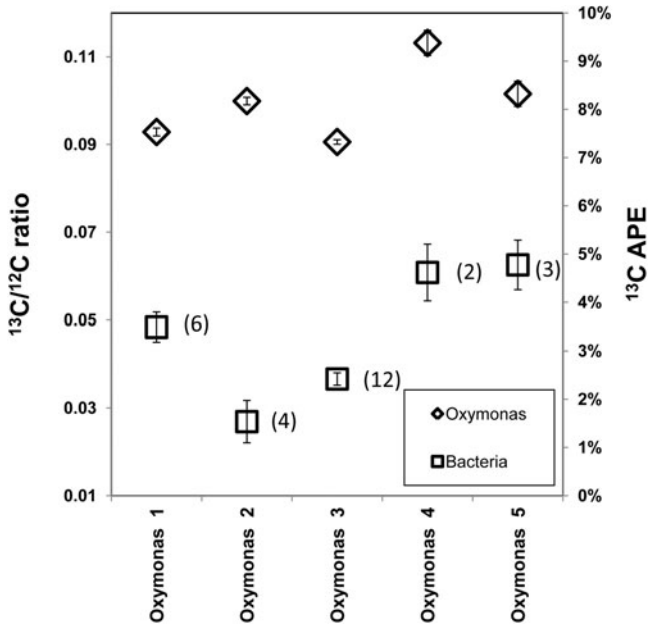

Figure 5. Comparison of ^{13}C enrichment ($^{13}C/^{12}C$ ratios and ^{13}C APE) for five *Oxymonas dimorpha* cells and their respective surface bacterial symbionts. Data are from ultramicrotome thin sections in which surface bacterial symbionts could be clearly identified. Sample sizes for bacteria are in parentheses. Error bars represent the standard error for individual *O. dimorpha* measurements, or the standard error of the mean for bacteria from an individual *O. dimorpha* cell. Control $^{13}C/^{12}C$ ~0.01.

pha cell itself was approximately one-fifth than that seen in whole cells, and much lower than measurements made of FIB-milled cells, presumably due to dilution caused by ^{12}C introduced during infiltration with the LR White resin (Fig. 4). NanoSIMS imaging provided resolution sufficient to clearly distinguish attached bacterial surface symbionts from the host *O. dimorpha* cell (Fig. 3C, arrows). This allowed us to draw ROIs around these bacterial cells using custom software (LIMAGE) to extract quantitative data on carbon isotopic ratios ($^{13}C/^{12}C$). It should be noted that TEM images (e.g., Fig. 3A) and NanoSIMS images (e.g., Figs. 3B, 3C) of a given section differ somewhat in that

NanoSIMS is a surface analytical technique showing ~5 nm worth of depth data, while TEM imaging in this case shows ~100–200 nm of depth data (i.e., the same depth as the thickness of the section). Also, as a result of the surface nature of the NanoSIMS image, grid bars that obscure the top and bottom of the cell with TEM imaging (Fig. 3A) are not visible (Figs. 3B, 3C). Isotopic data from NanoSIMS imaging of thin sections show that symbiotic surface bacteria associated with each of the five *O. dimorpha* cells were consistently and significantly less ^{13}C enriched than the interior of the *O. dimorpha* cells (Figs. 3B, 5).

Discussion

The combination of stable isotope tracers and high-resolution imaging mass spectrometry (nanoSIP) has provided a new means to link phylogeny and function in complex microbial communities (Behrens et al., 2008; Musat et al., 2008; Woebken et al., 2012). We have extended this general approach to protists and their bacterial surface symbionts, here providing evidence that an oxymonad protist from the hindgut of a lower termite phagocytoses and metabolizes cellulose, and may also provide carbon derived from this to its bacterial surface symbionts. Below we discuss the methodology developed to adapt nanoSIP for protists as well as the ecological hypotheses of our findings.

Fixation of Hindgut Microbes for SEM and NanoSIMS

The fixation procedure described here is successful at producing well-preserved whole protist and bacterial cells and resin-embedded cells for ultramicrotome sections that generally resist deformation while retaining the integrity of cell membranes and fine scale structures such as flagella, and surface symbiotic bacteria (Figs. 1A–1G). Free-swimming bacteria are also well preserved (Fig. 1C, arrows). This method is also compatible with the use of stable isotope tracers for analysis with NanoSIMS.

Thus, a single fixation is sufficient to provide material for examination by four different imaging modalities: SEM, FIB-SEM, TEM, and NanoSIMS. This is accomplished by splitting fixed material into approximately equal portions for subsequent processing for whole cell analysis and resin embedding. Additionally, the method requires relatively few reagents, and whole cells can be ready for examination within 1 day. The inability to positively identify some protists to the species level was not due to insufficient quality of preservation, but rather is due to the fact that for some species descriptions are old and based on LM alone, and because features necessary for positive identification cannot be seen in whole cells or with any single imaging modality (see Carpenter et al., 2011).

Specimen Preparation Techniques for NanoSIP

Sample preparation for nanoSIP poses a number of challenges, including exposing and identifying the target and making the sample sufficiently flat. The three methods of sample preparation—whole cell, FIB section, and ultramicrotome section—produced samples that can be analyzed by NanoSIMS to characterize the isotopic enrichment of the protists and bacteria. The major benefit of the whole cell approach is the ease of target identification. Examining whole cells affords a quick look at overall cell form, size, and often the arrangement and number of flagella and bacterial surface symbionts. These characters are often the most informative in taxonomic identifications of these organisms. By comparison, identification of protists in ultramicrotome sections relies on finding a plane of section showing enough characters for positive identification.

The whole cell method, however, has two downsides. One is that many of the protists are quite large (100 μm or more in one dimension) and some are nearly spherical in shape (e.g., *K. loriculata*). This topography affects the local ion extraction characteristics and did result in some areas having low ion yields (<10% of typical), which made analyses unreliable or entirely unfeasible. Topography can also prevent metal coating from connecting between the protist and the substrate, which may explain charging that was observed. In some cases, sputtering a large area with a high (>100 pA Cs^+) primary beam for a short period reduced charging and improved ion yield. Based on our control analyses, the key to reliable analyses was avoiding targets with low ion yields and closely monitoring instrument tuning, particularly individual mass peak shapes.

The second problem with whole cell analysis is that for protists with a dense covering of bacterial surface symbionts (e.g., *O. dimorpha*), it may not be possible to clearly differentiate between the bacteria at the surface and the protist below. We attempted depth profiling, but found that the differential sputtering of the bacteria on the surface of the protist, and of the protist itself, resulted in unacceptable topographic relief and significant uncertainty regarding whether the data were from the bacteria, the protist, or both. Therefore, we were unable to conclusively address one central question—the nutrient relationship between *O. dimorpha* and its associated bacteria—with this method. Therefore, the ecological interpretation below uses the FIB- and thin-section data.

Ultramicrotome sections of embedded material have the potential to allow unequivocal delineation between protist and surface symbionts (Fig. 3), as well as the ability to examine heterogeneity in intracellular isotopic enrichments (i.e., whether certain organelles become more enriched than others, or the cytosol, e.g., Fig. 3B). Examination of thin sections also eliminates topography issues. However, as mentioned above, identification of individual target cells becomes more challenging than with whole cells due to the fact that a favorable plane of section is necessary to see enough distinguishing characters. This in turn makes it difficult to identify enough cells for analysis, especially for small, rare members of the community (e.g., *Trichomonas* spp. in Fig. 1F). Our data suggest that carbon in the embedding resin can significantly dilute the ^{13}C tracer in the embedded cells (by roughly fivefold) (Fig. 4), though given

the high cell-to-cell variability and internal heterogeneity we observed, additional trials would be needed to precisely quantify this effect.

One key benefit of the FIB approach is that it maintains the ease of target identification provided by the whole cell approach, while enabling the bacteria and the protists to be clearly differentiated—i.e., by cleanly removing the top of the protist cell with attached bacteria, thus revealing its interior and intracellular heterogeneity in ^{13}C enrichment (Fig. 2). Certain areas inside FIB-cut cells show enrichments more than five times higher than those detected by depth profiling, reaching $^{13}C/^{12}C$ ratios of 4:1 or greater (^{13}C APE $>$ 79%; Figs. 2B, 2D, 4). FIB sectioning also reduces topographic effects. The major downside of the FIB approach is that it is significantly slower and more costly; it may require an entire day to top-cut four or five large cells.

Hypotheses for the Ecological/Functional Role of Oxymonads and Carbon Transfer to Bacterial Symbionts

The ecological roles and nutritional modes of oxymonads are poorly understood, and some species are thought to obtain nutrition from wood only indirectly—by absorbing metabolites produced by other members of the community, and not directly phagocytosing wood fragments (Cleveland, 1925; Kiuchi et al., 2004; Carpenter et al., 2008). However, in the case of *O. dimorpha*, the extremely high ^{13}C enrichment (4:1 $^{13}C/^{12}C$ ratio, ^{13}C APE ~79%) of relatively large areas (10 μm or larger)—some of which appear to be bounded by phagosomal membranes—observed in FIB-milled cells (Figs. 2B, 2D) and also in thin section (Fig. 3B), suggests that these areas represent phagocytosed ^{13}C cellulose material itself. The ability to form such large (>5 μm), irregularly shaped vesicles (phagosomes, as in Fig. 2C, arrow) to engulf food substances, as opposed to only small (<5 μm) globular-like structures (endosomes) has been shown to be correlated with wood digestion in hindgut protists of the termite *Reticulitermes speratus* Kolbe (Kiuchi et al., 2004). There is also evidence that the presence of cellulose is a requirement for engulfment of such particles (Yamaoka, 1979; Yoshimura, 1995). Taken together, this evidence suggests that *O. dimorpha* plays a role in the digestion of ingested wood fragments in the hindgut of *P. simplicicornis*. This result adds to other evidence (Kiuchi et al., 2004) that wood digestion is not a function of taxonomy—i.e., carried out only by certain members of Parabasalia—but rather of size, with the larger protists of both Oxymonadida and Parabasalia typically having the capacity to phagocytose and enzymatically degrade ingested wood fragments (Yoshimura, 1995; Yoshimura et al., 1996).

To date, hypotheses regarding the nature of metabolite exchange between termite gut protists and their symbiotic bacteria derive from two completed genomes of bacteria symbiotic with large cellulolytic parabasalid protist species (Hongoh et al., 2008*a*, 2008*b*). These data suggest that glucose derived from lignocellulose breakdown is transferred from the protist to its bacterial symbionts in exchange for essential nitrogenous compounds. However, to our knowledge, nothing is known about the nature of metabolite exchange between oxymonads and their bacterial symbionts. Our data suggest that at least *O. dimorpha* may act in a manner similar to certain large cellulolytic parabasalid protists by transferring carbon compounds derived from lignocelluose breakdown to its bacterial symbionts. We would argue that the consistently lower ^{13}C enrichments seen in the surface bacteria relative to the *O. dimorpha* cell interior, combined with evidence for cellulose degradation in *O. dimorpha* make this the most likely hypothesis. However, our data cannot exclude alternate hypotheses, such as the possibility that the surface bacteria of *O. dimorpha* may obtain some or all of their ^{13}C from some other source, e.g., directly from hindgut fluid. However, cellulolytic capability is not known from lower termite hindgut bacteria (e.g., Hongoh et al., 2008*a*, 2008*b*; Ohkuma & Brune, 2011), so it seems likely that the ultimate source of the ^{13}C would have to be from one of the (presumably larger species of) hindgut protists in the *P. simplicicornis* hindgut. Additional lines of evidence including genomic data and further experimental approaches—including possibly a timed series of isotopic labeling experiments with NanoSIMS—are needed to support or refute this hypothesis.

Previous research indicates that spirochetes in the termite hindgut have the ability to fix dinitrogen from air (Lilburn et al., 2001). Our SEM imaging reveals bacteria with spirochete-like morphology on the *O. dimorpha* surface (Fig. 2C), and we hypothesize that *O. dimorpha* may play a role in providing carbon compounds from lignocellulose degradation as well as a habitat for spirochetes contributing to nitrogen fixation and metabolism in the hindgut of *P. simplicicornis*. However, whether *O. dimorpha* receives nitrogenous nutrients from its surface symbionts remains unknown.

Conclusions

We have developed an effective method for direct, *in situ* stable isotope labeling of lower termite hindgut microbial communities (i.e., with ^{13}C-enriched cellulose) and subsequent fixation of this (or unlabeled) material, allowing for the culture-independent analysis of the ecological and functional roles of uncultivable microbes as well as protist–bacterial interactions. Protist and bacterial cells fixed with this method retain a high degree of overall structural and surface integrity and can be subsequently processed in three different ways for structural and isotopic imaging. Whole cell imaging enabled the easiest target identification, FIB milling provided the most reliable isotopic data for protist interiors, and thin sections provided the best samples for differentiating the isotopic composition of bacterial symbionts from that of the protist. This study represents one of the first successful efforts in using NanoSIMS to study interactions between protists and bacterial symbionts. Based on these analyses, we hypothesize that *O. dimorpha* is capable of digesting cellulose and transferring some of the derived car-

bon compounds to its bacterial surface symbionts. However, at this time we cannot rule out the alternative hypothesis that bacteria may obtain some or all of their carbon directly from hindgut fluid. The observation of putative phagosomes surrounding highly enriched material suggests that this protist is capable of engulfing cellulose and wood despite its dense coverage of bacteria. This approach can provide a direct line of evidence for formulating new hypotheses about protist ecology and cell biology, as well as testing hypotheses based on -omics, morphological, and other experimental data. More broadly, we believe these methods show promise for further culture-independent *in situ* investigations of a wide range of eukaryote–prokaryote symbioses, including host–pathogen and mutualistic interactions.

Acknowledgments

This work was supported by the Lawrence Livermore National Laboratory Laboratory Directed Research and Development program (011-LW-039) and the Department of Energy OBER LLNL Biofuels Scientific Focus Area (SFA) program (SCW1039). Work at LLNL was performed under the auspices of the US Department of Energy under contract DE-AC52-07NA27344. The authors thank Ian Hutcheon for guidance, Christina Ramon and Nick Teslich of LLNL for technical assistance, and Sarah E. Baker (LLNL), Moriya Ohkuma (RIKEN Bioresource Center, Wako-Saitama, Japan), Andreas Brune (Max Planck Institute for Terrestrial Microbiology, Marburg, Germany), and Brian Leander (University of British Columbia) and Elaine Humphrey (University of Victoria, Canada) for helpful discussions and other assistance.

References

Behrens, S., Losekann, T., Pett-Ridge, J., Weber, P.K., Ng, W.O., Stevenson, B.S., Hutcheon, I.D., Relman, D.A. & Spormann, A.M. (2008). Linking microbial phylogeny to metabolic activity at the single-cell level by using enhanced element labeling-catalyzed reporter deposition fluorescence in situ hybridization (EL-FISH) and NanoSIMS. *Appl Environ Microbiol* **74**(10), 3143–3150.

Berchtold, M., Chatzinotas, A., Schönhuber, W., Brune, A., Amann, R., Hahn, D. & König, H. (1999). Differential enumeration and *in situ* localization of microorganisms in the hindgut of the lower termite *Mastotermes darwinensis* by hybridization with rRNA-targeted probes. *Arch Microbiol* **172**, 407–416.

Bloodgood, R.A. & Fitzharris, T.P. (1976). Specific associations of prokaryotes with symbiotic flagellate protozoa from the hindgut of the termite Reticulitermes and the wood-eating roach Cryptocercus. *Cytobios* **17**(66), 103–122.

Boschker, H.T.S., Nold, S.C., Wellsbury, P., Bos, D., de Graaf, W., Pel, R., Parkes, R.J. & Cappenberg, T.E. (1998). Direct linking of microbial populations to specific biogeochemical processes by C-13-labelling of biomarkers. *Nature* **392**(6678), 801–805.

Brugerolle, G. & Bordereau, C. (2004). The flagellates of the termite *Hodotermopsis sjoestedti* with special reference to Hoplonympha, Holomastigotes and Trichomonoides trypanoides n. comb. *Eur J Protistol* **40**, 163–174.

Brugerolle, G. & Lee, J.H. (2000*a*). Order oxymonadida. In *The Illustrated Guide to the Protozoa*, 2nd ed., Lee, J.J., Leedale, G.F. & Bradbury, P. (Eds.), pp. 1186–1195. Lawrence, KS: Allen Press, Inc.

Brugerolle, G. & Lee, J.J. (2000*b*). Phylum Parabasalia. In *An Illustrated Guide to the Protozoa*, 2nd ed., Lee, J.J., Leedale, G.F. & Bradbury, P. (Eds.), pp. 1196–1250. Lawrence, KS: Allen Press Inc.

Brune, A. & Ohkuma, M. (2011). Role of the termite gut microbiota in symbiotic digestion. In *Biology of Termites: A Modern Synthesis*, Bignell, D.E., Roisin, Y. & Lo, N. (Eds.), pp. 439–475. London: Springer.

Brune, A. & Stingl, U. (2006). Prokaryotic symbionts of termite gut flagellates: Phylogenetic and metabolic implications of a tripartite symbiosis. *Prog Mol Subcell Biol* **41**, 39–60.

Carpenter, K.J., Chow, L. & Keeling, P.J. (2009). Morphology, phylogeny, and diversity of Trichonympha (Parabasalia: Hypermastigida) of the wood-feeding cockroach *Cryptocercus punctulatus*. *J Eukaryot Microbiol* **56**(4), 305–313.

Carpenter, K.J., Horak, A., Chow, L. & Keeling, P.J. (2011). Symbiosis, morphology, and phylogeny of Hoplonymphidae (Parabasalia) of the wood-feeding roach *Cryptocercus punctulatus*. *J Eukaryot Microbiol* **58**(5), 426–436.

Carpenter, K.J., Horak, A. & Keeling, P.J. (2010). Phylogenetic position and morphology of spirotrichosomidae (parabasalia): New evidence from Leptospironympha of *Cryptocercus punctulatus*. *Protist* **161**(1), 122–132.

Carpenter, K.J. & Keeling, P.J. (2007). Morphology and phylogenetic position of *Eucomonympha imla* (Parabasalia: Hypermastigida). *J Eukaryot Microbiol* **54**(4), 325–332.

Carpenter, K.J., Waller, R.F. & Keeling, P.J. (2008). Surface morphology of *Saccinobaculus* (Oxymonadida): Implications for character evolution and function in oxymonads. *Protist* **159**(2), 209–221.

Cleveland, L.R. (1925). The effects of oxygenation and starvation on the symbiosis between the termite Termopsis and its intestinal flagellates. *Biol Bull* **48**, 309–325.

Cleveland, L.R. & Grimstone, A.V. (1964). The fine structure of the flagellate *Mixotricha paradoxa* and its associated microorganisms. *Proc R Soc* **159**, 668–686.

Cleveland, L.R., Hall, S.R., Sanders, E.P. & Collier, J. (1934). The wood-feeding roach *Cryptocercus*, its protozoa, and the symbiosis between protozoa and roach. *Mem Am Acad Arts Sci* **17**, 1–342.

Giberson, R.T., Demaree, R.S. & Nordhausen, R.W. (1997). Four hour processing of clinical/diagnostic specimens for electron microscopy using microwave technique. *J Vet Diag Invest* **9**, 61–67.

Grassi, B. (1917). Flagellati viventi nei Termiti. *Mem R Accad Lincei* **12**(5), 331–394.

Hollande, A. & Carruette-Valentin, J. (1971). Les atractophores, l'induction du fuseau et la division cellulaire chez les Hypermastigines Étude infrastructurale et révision systématique desTrichonymphines et des Spirotrichonymphines. *Protistologica* **7**, 5–100.

Hollande, A. & Valentin, J. (1968). Infrastructure du complexe rostral et origine du fuseau chez Staurojoenina caulleryi. *Comptes Rendus Hebdomadaires des Seances de l'academie de sciences Series D* **266**, 1283–1286.

Hongoh, Y., Ohkuma, M. & Kudo, T. (2003). Molecular analysis of bacterial microbiota in the gut of the termite *Reticulitermes speratus* (Isoptera: Rhinotermitidae). *FEMS Microbiol Ecol* **44**(2), 231–242.

Hongoh, Y., Sharma, V.K., Prakash, T., Noda, S., Taylor, T.D., Kudo, T., Sakaki, Y., Toyoda, A., Hattori, M. & Ohkuma, M. (2008*a*). Complete genome of the uncultured termite group 1 bacteria in a single host protist cell. *Proc Natl Acad Sci USA* **105**(14), 5555–5560.

Hongoh, Y., Sharma, V.K., Prakash, T., Noda, S., Toh, H., Taylor, T.D., Kudo, T., Sakaki, Y., Toyoda, A., Hattori, M. & Ohkuma, M. (2008*b*). Genome of an endosymbiont coupling N_2 fixation to cellulolysis within protist cells in termite gut. *Science* **322**(5904), 1108–1109.

Inward, D., Beccaloni, G. & Eggleton, P. (2007). Death of an order: A comprehensive molecular phylogenetic study confirms that termites are eusocial cockroaches. *Biol Lett* **3**(3), 331–335.

Kirby, H. (1926). On *Staurojoenina assimilis* sp. nov. an intestinal flagellate from the termite Kalotermes minor Hagen. *Univ Calif Publ Zool* **29**, 25–102.

Kirby, H. (1932). Flagellates of the genus Trichonympha in termites. *Univ Calif Publ Zool* **37**, 349–476.

Kiuchi, I., Moriya, S. & Kudo, T. (2004). Two different size-distributions of engulfment-related vesicles among symbiotic protists of the lower termites, *Reticulitermes speratus*. *Microb Environ* **19**, 211–214.

Koidzumi, M. (1921). Studies on the intestinal protozoa found in the termites of Japan. *Parasitol* **13**, 235–309.

Leadbetter, J.R., Schmidt, T.M., Graber, J.R. & Breznak, J.A. (1999). Acetogenesis from H_2 plus CO_2 by spirochetes from termite guts. *Science* **283**(5402), 686–689.

Leander, B.S. & Keeling, P.J. (2004). Symbiotic innovation in the oxymonad *Streblomastix strix*. *J Eukaryot Microbiol* **51**(3), 291–300.

Lechene, C., Hillion, F., McMahon, G., Benson, D., Kleinfeld, A.M., Kampf, J.P., Distel, D., Luyten, Y., Bonventre, J., Hentschel, D., Park, K.M., Ito, S., Schwartz, M., Benichou, G. & Slodzian, G. (2006). High-resolution quantitative imaging of mammalian and bacterial cells using stable isotope mass spectrometry. *J Biol* **5**(6), 20.

Leidy, J. (1877). On intestinal parasites of *Termes flavipes*. *Proc Acad Nat Sci Philadelphia* **29**, 146–149.

Lilburn, T.G., Kim, K.S., Ostrom, N.E., Byzek, K.R., Leadbetter, J.R. & Breznak, J.A. (2001). Nitrogen fixation by symbiotic and free-living spirochetes. *Science* **292**(5526), 2495–2498.

Lo, N., Tokuda, G., Watanabe, H., Rose, H., Slaytor, M., Maekawa, K., Bandi, C. & Noda, H. (2000). Evidence from multiple gene sequences indicates that termites evolved from wood-feeding cockroaches. *Curr Biol* **10**(13), 801–804.

Maaß, A. & Radek, R. (2006). The gut flagellate community of the termite *Neotermes cubanus* with special reference to *Staurojoenina* and *Trichovina hrdyi* nov. gen. nov. sp. *Eur J Protistol* **42**, 125–141.

Manefield, M., Whiteley, A.S., Griffiths, R.I. & Bailey, M.J. (2002). RNA stable isotope probing, a novel means of linking microbial community function to phylogeny. *Appl Environ Microbiol* **68**(11), 5367–5373.

Mayali, X., Weber, P.K., Brodie, E.L., Mabery, S., Hoeprich, P.D. & Pett-Ridge, J. (2012). High-throughput isotopic analysis of RNA microarrays to quantify microbial resource use. *ISME J* **6**, 1210–1221.

Miller, M. (1969). Caste differentiation in lower termites. In *Biology of Termites*, Krishna, K. and Weesner, F. (Eds.), pp. 283–307. New York: Academic Press.

Murrell, J.C. & Whiteley, A.S. (Eds.) (2011). *Stable Isotope Probing and Related Technologies*. Washington, DC: ASM Press.

Musat, N., Halm, H., Winterholler, B., Hoppe, P., Peduzzi, S., Hillion, F., Horreard, F., Amann, R., Jorgensen, B.B. & Kuypers, M.M.M. (2008). A single-cell view on the ecophysiology of anaerobic phototrophic bacteria. *Proc Natl Acad Sci USA* **105**(46), 17861–17866.

Nakashima, K.I., Watanabe, H. & Azuma, J.I. (2002). Cellulase genes from the parabasalian symbiont *Pseudotrichonympha grassii* in the hindgut of the wood-feeding termite *Coptotermes formosanus*. *Cell Mol Life Sci* **59**(9), 1554–1560.

Noda, S., Iida, T., Kitade, O., Nakajima, H., Kudo, T. & Ohkuma, M. (2005). Endosymbiotic Bacteroidales bacteria of the flagellated protist *Pseudotrichonympha grassii* in the gut of the termite *Coptotermes formosanus*. *Appl Environ Microbiol* **71**(12), 8811–8817.

Noda, S., Inoue, T., Hongoh, Y., Kawai, M., Nalepa, C.A., Vongkaluang, C., Kudo, T. & Ohkuma, M. (2006). Identification and characterization of ectosymbionts of distinct lineages in Bacteroidales attached to flagellated protists in the gut of termites and a wood-feeding cockroach. *Environ Microbiol* **8**(1), 11–20.

Ohkuma, M. (2003). Termite symbiotic systems: Efficient bio-recycling of lignocellulose. *Appl Microbiol Biotechnol* **61**(1), 1–9.

Ohkuma, M. & Brune, A. (2011). Diversity, structure, and evolution of the termite gut microbial community. In *Biology of Termites: A Modern Synthesis*, Bignell, D.E., Roisin, Y. & Lo, N. (Eds.), pp. 413–438. London: Springer.

Ohkuma, M. & Kudo, T. (1996). Phylogenetic diversity of the intestinal bacterial community in the termite *Reticulitermes speratus*. *Appl Environ Microbiol* **62**(2), 461–468.

Ohkuma, M., Sato, T., Noda, S., Ui, S., Kudo, T. & Hongoh, Y. (2007). The candidate phylum "Termite Group 1" of bacteria: Phylogenetic diversity, distribution, and endosymbiont members of various gut flagellated protists. *FEMS Microbiol Ecol* **60**(3), 467–476.

Pett-Ridge, J. & Weber, P. (2012). NanoSIP: NanoSIMS applications for microbial biology. In *Microbial Systems Biology: Methods and Protocols*, Navid, A. (Ed.), pp. 375–408. New York: Humana Press.

Popa, R., Weber, P.K., Pett-Ridge, J., Finzi, J.A., Fallon, S.J., Hutcheon, I.D., Nealson, K.H. & Capone, D.G. (2007). Carbon and nitrogen fixation and metabolite exchange in and between individual cells of *Anabaena oscillarioides*. *ISME J* **1**(4), 354–360.

Radajewski, S., Ineson, P., Parekh, N.R. & Murrell, J.C. (2000). Stable-isotope probing as a tool in microbial ecology. *Nature* **403**(6770), 646–649.

Radek, R., Hausmann, K. & Breunig, A. (1992). Ectobiotic and endocytobiotic bacteria associated with the termite flagellate Joenia-Annectens. *Acta Protozoologica* **31**(2), 93–107.

Rother, A., Radek, R. & Hausmann, K. (1999). Characterizaion of surface structures covering termite flagellates of the family oxymonadidae and ultrastructure of two oxymonad species, *Microrhopalodina multinucleata* and *Oxymonas* sp. *Eur J Protistol* **35**, 1–16.

Stingl, U., Maass, A., Radek, R. & Brune, A. (2004). Symbionts of the gut flagellate *Staurojoenina* sp. from *Neotermes cubanus* represent a novel, termite-associated lineage of Bacteroidales: Description of "Candidatus Vestibaculum illigatum". *Microbiol* **150**(Pt 7), 2229–2235.

Trager, W. (1934). The cultivation of a cellulose-digesting flagellate, *Trichomonas termopsidis*, and of certain other termite protozoa. *Biol Bull* **66**, 182–190.

Weber, P.K., Graham, G.A., Teslich, N.E., Chan, W.M., Ghosal, S., Leighton, T.J. & Wheeler, K.E. (2010). NanoSIMS imaging of Bacillus spores sectioned by focused ion beam. *J Microsc* **238**(3), 189–199.

Woebken, D., Burow, L.C., Prufert-Bebout, L., Bebout, B.M., Hoehler, T.M., Pett-Ridge, J., Spormann, A.M., Weber, P.K. & Singer, S.W. (2012). Identification of a novel cyanobacterial group as active diazotrophs in a coastal microbial mat using NanoSIMS analysis. *ISME J* **6**, 1427–1439.

Yamaoka, I. (1979). Selective ingestion of food by the termite protozoa, *Trichonympha agilis*. *Zoolog Mag (Tokyo)* **88**, 174–179.

Yamin, M.A. (1979). Flagellates of the orders *Trichomonadida Kirby*, *Oxymonadida Grasse*, and *Hypermastigida Grassi* and *Foa* reported from lower termites (Isoptera families Mastotermitidae, Kalotermitidae, Hodotermitidae, Termopsidae, Rhinotermitidae, and Serritermitidae) and from the wood-feeding roach cryptocercus (Dictyoptera, Cryptocercidae). *Sociobiology* **4**(1), 3–119.

Yamin, M.A. (1981). Cellulose metabolism by the flagellate trichonympha from a termite is independent of endosymbiotic bacteria. *Science* **211**(4477), 58–59.

Yoshimura, T. (1995). Contribution of the protozoan fauna to nutritional physiology of the lower termite *Coptotermes formosanus* Shiraki (Isoptera: Rhinotermitidae). *Wood Res* **82**, 68–129.

Yoshimura, T., Fujino, T., Itoh, T., Tsunodo, K. & Takahashi, M. (1996). Ingestion and decomposition of wood and cellulose by the protozoa in the hindgut of *Coptotermes formosanus* Shiraki (Isoptera: Rhinotermitidae) as evidenced by polarizing and transmission electron microscopy. *Holzforschung* **50**, 99–104.